

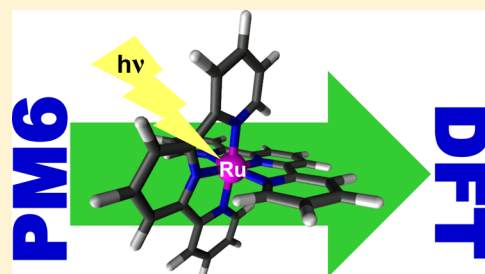
# Predicting Structures of Ru-Centered Dyes: A Computational Screening Tool

Lisa A. Fredin\* and Thomas C. Allison

Chemical Informatics Research Group, Chemical Science Division, Material Measurement Laboratory, National Institute of Standards and Technology, 100 Bureau Drive, Stop 8320, Gaithersburg, Maryland 20899-8320, United States

## Supporting Information

**ABSTRACT:** Dye-sensitized solar cells (DSCs) represent a means for harvesting solar energy to produce electrical power. Though a number of light harvesting dyes are in use, the search continues for more efficient and effective compounds to make commercially viable DSCs a reality. Computational methods have been increasingly applied to understand the dyes currently in use and to aid in the search for improved light harvesting compounds. Semiempirical quantum chemistry methods have a well-deserved reputation for giving good quality results in a very short amount of computer time. The most recent semiempirical models such as PM6 and PM7 are parametrized for a wide variety of molecule types, including organometallic complexes similar to DSC chromophores. In this article, the performance of PM6 is tested against a set of 20 molecules whose geometries were optimized using a density functional theory (DFT) method. It is found that PM6 gives geometries that are in good agreement with the optimized DFT structures. In order to reduce the differences between geometries optimized using PM6 and geometries optimized using DFT, the PM6 basis set parameters have been optimized for a subset of the molecules. It is found that it is sufficient to optimize the basis set for Ru alone to improve the agreement between the PM6 results and the DFT results. When this optimized Ru basis set is used, the mean unsigned error in Ru–ligand bond lengths is reduced from 0.043 to 0.017 Å in the set of 20 test molecules. Though the magnitude of these differences is small, the effect on the calculated UV/vis spectra is significant. These results clearly demonstrate the value of using PM6 to screen DSC chromophores as well as the value of optimizing PM6 basis set parameters for a specific set of molecules.



## INTRODUCTION

Harvesting energy from solar sources is prominent and enticing in the spectrum of renewable energy sources currently being used, developed, and investigated because of solar energy's high flux in many locations.<sup>1</sup> Dye-sensitized solar cells (DSCs) represent a promising area of current investigation due to their well-defined chemistry and stability.<sup>2</sup> However, current state-of-the-art light-harvesting dyes are too costly per unit energy output, leading to a hunt for chromophores with higher efficiency. Metal-centered dye complexes, such as Ru(II)- or Fe(II)-containing compounds, or metal porphyrins, provide high DSC efficiencies due to their highly favorable excited state properties. Ligand field theory states that the coordination geometry and electron density on the metal center control the redox and excited state properties of metal-centered chromophores. Ru(II)–polypyridyl complexes have led to some of the highest measured DSC efficiencies to date<sup>3</sup> due to the alignment of their excited states with the titania conduction band and favorable redox properties.

Much attention over the past few decades has been focused on finding polypyridyl tris-bidentate and bis-tridentate Ru(II) complexes to improve solar conversion efficiencies.<sup>4–9</sup> Tris-bidentate complexes like  $[\text{Ru}(\text{BPy})_3]^{2+}$  (BPy = 2,2'-bipyridine) showed early promise having long (ns) room-temperature excited state lifetimes.<sup>10</sup> However, the  $C_2$  axis in *meridional* bis-

tridentate complexes like  $[\text{Ru}(\text{TPy})_2]^{2+}$  (TPy = 2,2':6',2''-terpyridine)<sup>11,12</sup> allow for ordered packing of structures and more rigid coordination geometry, leading to more stable structures. An advantage of these polypyridyl ligands is that they can be tuned through the addition of substituents to the ligand backbone.<sup>10</sup> Ligand field theory predicts that the electron donating or withdrawing nature of these substituents and their location affects the electronic density on the metal,<sup>13–16</sup> where greater electron density leads to larger ligand field splitting and therefore to higher energy excited states. Predictably, every promising ligand backbone has led to many substituted structures. Substitutions in the 4 and 4' positions<sup>10,17</sup> are most common due to the steric hindrance at 3 and 3' positions<sup>18</sup> that make these complexes hard to synthesize and due to the bad performance observed for many 5 and 5' substitutions.<sup>19</sup> While carboxyl groups are the most commonly used substituents as they provide linker points to attach molecules to oxide surfaces like titania, many substituents have been proposed, e.g., amines, furans, ketones, and hydroxyl. While the electronic effects of substituents often provide fine-tuning, the electron density on the metal can be

Received: January 27, 2016

Revised: March 4, 2016

Published: March 16, 2016

Table 1. List of 20 Ru-Containing DSC Molecules Used in Optimizing and Testing a New PM6 Basis Set for Ru

name	formula	name	formula
training set			
Ru(DQP) <sub>2</sub>	[Ru(DQP) <sub>2</sub> ] <sup>2+</sup>	N3	[Ru(BPy-2COOH) <sub>2</sub> (NCS) <sub>2</sub> ]
Ru(DBPzP) <sub>2</sub>	[Ru(DBPzP) <sub>2</sub> ] <sup>2+</sup>	Ru(PzPyPz) <sub>2</sub>	[Ru(PzPyPz) <sub>2</sub> ] <sup>2+</sup>
Ru(DQPz) <sub>2</sub>	[Ru(DQPz) <sub>2</sub> ] <sup>2+</sup>	Ru(TPy) <sub>2</sub>	[Ru(TPy) <sub>2</sub> ] <sup>2+</sup>
testing set			
Ru(NCN) <sub>2</sub>	[Ru(NCN) <sub>2</sub> ]	Ru(DQPFur) <sub>2</sub>	[Ru(DQPFur) <sub>2</sub> ] <sup>2+</sup>
black	[Ru(TPy-COOH)(NCS) <sub>3</sub> ] <sup>3-</sup>	Ru(DQPl) <sub>2</sub>	[Ru(DQPl) <sub>2</sub> ] <sup>2+</sup>
Ru(DNinP) <sub>2</sub>	[Ru(DNinP) <sub>2</sub> ] <sup>2+</sup>	Ru(DQPNH <sub>2</sub> ) <sub>2</sub>	[Ru(DQPl) <sub>2</sub> ] <sup>2+</sup>
Ru(DQB) <sub>2</sub>	[Ru(DQB) <sub>2</sub> ]	Ru(CPyC)(TPy)	[Ru(CPyC)(TPy)] <sup>2+</sup>
Ru(BPy) <sub>3</sub>	[Ru(BPy) <sub>3</sub> ] <sup>2+</sup>	Ru(DQxP) <sub>2</sub>	[Ru(DQxP) <sub>2</sub> ] <sup>2+</sup>
Ru(DQIm) <sub>2</sub>	[Ru(DQIm) <sub>2</sub> ] <sup>2+</sup>	Ru(PzbPybPz) <sub>2</sub>	[Ru(PzbPybPz) <sub>2</sub> ] <sup>2+</sup>
Ru(DQPCCOOH) <sub>2</sub>	[Ru(DQPCCOOH) <sub>2</sub> ] <sup>2+</sup>	Ru(DCpP) <sub>2</sub>	[Ru(DCpP) <sub>2</sub> ] <sup>2+</sup>

increased by replacing the pyridyl coordination with cyclo-metalated groups or carbenes.<sup>16,20–25</sup> In addition, changes in the coordination geometry have a much larger effect on lifetimes due to changes in the relative energies of the metal-to-ligand charge transfer (MLCT) state and the metal-centered state (MC) in the triplet excited-state manifold. Ligand field theory predicts favorable properties with more octahedral geometries, driving exploration of expanded chelate rings, particularly 6-membered Ru–ligand chelates. The most striking example of this was the introduction of two 8-quinolinyl groups with a pyridine ring to form the tridentate ligand 2,6-di(8-quinolin-8-yl)pyridine (DQP),<sup>23</sup> which extended the excited state lifetime  $\approx 4$  orders of magnitude compared to [Ru(TPy)<sub>2</sub>]<sup>2+</sup>. These expanded coordination cage structures are often driven through the incorporation of heterocycles into the backbone,<sup>22,26</sup> like that of 8-quinolines<sup>23</sup> or pyrazoles.<sup>27</sup> The resulting active space of thousands of possible molecules has led to many promising results and many more complexes left to explore.

Computational approaches have considerable value in screening candidate dye molecules that may be difficult or time-consuming to synthesize and test for efficacy. Additionally, knowledge of the fundamental physics and chemistry that determines dye performance can aid in the *in silico* design of new dye molecules. Owing to the particularly good match between density functional theory (DFT) and time-dependent DFT (TD-DFT) calculations and the crystal structures and absorption spectra for a wide range of molecular systems,<sup>28–31</sup> DFT is frequently used to explain differences in measured DSC performance.<sup>25,26,32</sup> Typically, these calculations focus on the ground state geometry and vertical excited states from this geometry.<sup>26</sup> The optimized ground state minimum energy geometry allows us to study the ligand binding motif, coordination geometry, and electronic structure, all of which are related to the ligand field splitting and can provide insight into the photochemical properties of a complex in relation to well-studied chromophores. After confirming favorable ground state structures, the UV/vis spectrum (vertical excited states) of the molecule and optimization of multiple spin multiplicities provide valuable information about the interplay between excited states, complementing experimental studies.<sup>23,25–27,33</sup> These calculations, particularly when relaxed higher spin states are included, can be very time-consuming and therefore should be saved for molecules that already show particular promise. In contrast, in order to screen many light harvesting molecules for applications like DSCs, a fast and robust computational method is desirable, pointing to semiempirical alternatives.

Performing computations with accuracy and efficiency is of key importance in screening large sets of molecules *a priori*. Traditional semiempirical quantum chemistry methods (e.g., AM1,<sup>34</sup> PM3,<sup>35</sup> PM6,<sup>36</sup> PM7<sup>37</sup>) are widely used throughout the chemical community. These methods provide results that can be remarkably accurate and are produced with very low computational cost versus *ab initio* and DFT methods. Among the approximations used in semiempirical methods are the use of minimal basis sets and the neglect of certain classes of integrals. The loss of accuracy due to these approximations is typically recovered through parametrization against experimental data, leading to a method that is robust across a wide range of chemistries. However, if the training set is incomplete, certain interactions may not be well represented in the semiempirical model. It may also be possible to achieve improved results for a family of molecules by optimizing the PM6 basis set parameters for that family.

Here we employ PM6, which was parametrized with a number of group VIII metal complexes, including porphyrin structures.<sup>36</sup> The performance of PM6 in predicting the optimized structures of Ru-containing DSC molecules is studied by comparing PM6-optimized structures to DFT-optimized structures, which have been shown to accurately reproduce the observed crystal structures of rigid octahedral Ru(II) complexes.<sup>10,11,23</sup> While it is expected that PM6 optimizations of Ru(II)–polypyridyl complexes should be quite reasonable, since the metal porphyrins in the training set are also composed of metal–N or –C bonds, small differences in metal–ligand bond distances and in the octahedrality around the metal center (as measured by the metal–ligand inner-sphere bond angles) are known to affect the ligand field splitting in these types of chromophores. Therefore, it is desirable to explore optimization of specialized parameter sets for specific classes of compounds in a systematic manner, possibly improving the agreement between PM6-optimized structures and DFT-optimized structures, by a reparametrization of the PM6 basis set parameters. In this article, a set of Ru(II) DSC complexes is screened for favorable octahedrality, a Ru basis set for PM6 is optimized, and a universal method for PM6 basis set reparametrization for a specified set of molecules is reported. Significant improvements to the electronic structure (e.g., HOMO–LUMO gaps, UV/vis spectra) when using an optimized basis set are demonstrated.

## METHOD

**Training and Testing Set Selection.** A set of 20 Ru(II)-centered dyes (listed in Table 1) was chosen to span

representative complex and bonding types. The set includes tris-bidentate, bis-tridentate, homoleptic, and heteroleptic complexes, utilizing monodentate, polypyridyl, cyclometalated, and carbene ligands with pyrazole, pyridine, benzoyl, pyrrole, imidazole, quinoline, quinoxaline, and N-heterocyclic carbene subunits. The largest group of Ru(II) dyes uses polypyridyl ligands that bind to the Ru center via Ru–N bonds. The two tris-bidentate complexes in the set are Ru(BPy)<sub>3</sub><sup>38</sup> and N3 (*cis*-bis(isothiocyanato)bis(2,2′-bipyridyl-4,4′-dicarboxylato-ruthenium(II))).<sup>3,39</sup> The tridentate N3 derivative black dye<sup>40</sup> (tris(thiocyanato)-2,2′:6′,2′′-terpyridine-4,4′,4′′-tricarboxylato-ruthenium(II)) was also included; these both use conjugated polypyridyl ligands in conjunction with thiocyanato (NCS) monodentate ligands. In addition, homoleptic *meridional* bis-tridentate complexes incorporated are Ru(TPy)<sub>2</sub>,<sup>41</sup> Ru(PzPyPz)<sub>2</sub> (PzPyPz = 2,6-di(pyrazol-1-yl)pyridine, sometimes called bpp),<sup>42</sup> Ru(DBPzP)<sub>2</sub> (DBPzP = 2,6-dibenzopyrazolopyridine),<sup>43</sup> Ru(DQP)<sub>2</sub>,<sup>23</sup> and its 4-substituted analogues Ru(DQPCOOH)<sub>2</sub>,<sup>44</sup> Ru(DQPFur)<sub>2</sub>, and Ru(DQPNH<sub>2</sub>)<sub>2</sub>.<sup>44</sup> These are combined with other expanded cage compounds that employ both saturated, Ru(PzbPybPz)<sub>2</sub> (PzbPybPz = 2,6-di(pyrazol-1-ylmethyl)pyridine)<sup>45</sup> and Ru(DCpP)<sub>2</sub> (DCpP = 6-*bis*(2-carboxypyridyl)pyridine),<sup>46</sup> and aromatic, Ru(DNinP)<sub>2</sub> (DQinP = 2,6-di(N-7-azaindol-1-yl)pyridine),<sup>26</sup> extensions between the central and terminal rings. In addition, the strain in ligands can be reduced by reducing some of the aromatic rings from six-membered rings to five like in Ru(DQxP)<sub>2</sub> (DQxP = 2,6-di(quinoxalin-5-yl)pyridine),<sup>26</sup> Ru(DQPz)<sub>2</sub> (DQPz = 1,3-bis(8-quinolinyl)pyrazole),<sup>47</sup> and Ru(DQPl)<sub>2</sub> (DQPl = 1,3-bis(8-quinolinyl)pyrrole). This extensive set of complexes gives a broad representation of ligands incorporating Ru–N bonding. In addition, Ru–C bound complexes were chosen including cyclometalated derivatives of TPy and DQP, Ru(NCN)<sub>2</sub> (NCN = dipyridylbenzene)<sup>48</sup> and Ru(DQB)<sub>2</sub> (DQB = 1,3-diquinolin-8-ylbenzene),<sup>49</sup> respectively. Finally, carbene homoleptic Ru(DQIm)<sub>2</sub> (DQIm = 1,3-bis(8-quinolinyl)-imidazole), and heteroleptic Ru(CPyC) (TPy) (CPyC = 2′,6′-bis(1-mesityl-3-methyl-1,2,3-triazol-4-yl-5-idene)-pyridine)<sup>20</sup> complexes are also represented.

This set of 20 DSC molecules was created to serve as a testing set. For each of the molecules, a set of important internal coordinates was defined. These coordinates included bond lengths and bond angles in the inner-sphere Ru–ligand bonding that best describe the critical structure of the DSC chromophore that determines its performance. From this set of 20 molecules, a subset of six molecules (the “training set”) was selected for use in optimizing the basis set parameters. This subset was chosen to represent some of the different types of chemical bonding seen in the testing set, especially featuring molecules for which the DFT geometries are known to match their experimental crystal structure well. Even though no compounds containing Ru–C bonds were included in the training set, the optimized PM6 was able to improve the match to the DFT for these structures. The list of molecules is presented in Table 1.

**DFT Calculations.** DFT geometries are known to reproduce the crystal structures of polypyridyl–Ru(II) complexes well,<sup>26,30,39,41,44,46,50</sup> and PBE0 has been found to give the best match to the crystal structure for the Ru(II) complexes of interest.<sup>51</sup> For consistency across complexes, we compare to the DFT-optimized geometries. Geometry optimizations of the 20 DSC molecules were carried out using the PBE0 functional<sup>52,53</sup> with the 6-31G(d,p) basis set for

all light atoms (H, C, N, O, and S), and the Stuttgart/Dresden (SDD) effective core potential (ECP) basis set<sup>54</sup> on Ru, with a polarizable continuum model (PCM) of acetonitrile (CH<sub>3</sub>CN) as the solvent.<sup>55</sup> Benchmarking has shown that this level of theory reproduces the crystal geometry well and that other levels of theory do not further improve agreement with the experimental geometry.<sup>56</sup> Geometries were fully optimized at the stated level of theory, and all structures were verified to be minima on their respective potential energy surfaces by ensuring that all of the vibrational frequencies were real valued.

UV/vis spectra were calculated using time-dependent DFT (TD-DFT), which is known to give good agreement with the experimental spectra.<sup>26,44</sup> Calculations are made based on PM6 and DFT optimized geometries. The calculated spectra are broadened using Lorentzian line shapes with widths of 0.2 eV. All calculations were carried out using the Gaussian 09 computational chemistry package.<sup>57</sup>

**Basis Set Reparametrization.** The process of producing new PM6 basis set parameters is based on optimization of the published PM6 parameters and hence is termed “reparametrization”. The Broyden–Fletcher–Goldfarb–Shanno (BFGS) method<sup>58</sup> was used to optimize the PM6 basis set parameters with respect to the set of selected coordinates for the molecules in the training set. The objective function ( $\epsilon$ ) is the normalized, weighted, mean of the squared values of the deviation of the PM6-optimized internal coordinate value from the DFT-optimized value of the coordinate

$$\epsilon = \frac{1}{n} \sum_{i=1}^n [w_i N_i (v_i^{\text{PM6}} - v_i^{\text{DFT}})]^2 \quad (1)$$

where  $n$  is the number of coordinates,  $i$  represents a particular coordinate,  $w_i$  is a weight factor for coordinate  $i$ ,  $N_i$  is a coordinate-type specific normalization factor, and  $v_i^\alpha$  is the value of a particular internal coordinate ( $\alpha = \text{PM6, DFT}$ ). The internal coordinates used were the inner-sphere bond lengths and bond angles around the Ru center. For each complex, the set of 6 Ru–ligand bond lengths and 12 octahedral bond angles (in an ideal octahedron 90°) form the optimization set for each complex. This is thus a redundant set of coordinates, not unlike those used in geometry optimization. In particular, it is overdetermined in bond angles, some of which are correlated depending on the ligand binding.

The BFGS method requires first derivatives to be computed. In the present case, these are derivatives of the objective function with respect to a change in the value of an internal coordinate taken from a PM6-optimized geometry. The derivatives were computed numerically using a two-point finite difference formula. Each time the objective function was evaluated, an optimization of the geometry of each molecule in the training set was performed using the PM6 method with a trial set of basis set parameters. Each time the gradient was evaluated, the objective function was evaluated for two small displacements of each of the basis set parameters that were being optimized. As basis set parameters were modified, it was not uncommon for a PM6 calculation to fail, typically due to problems with SCF convergence. When this occurred, a penalty value was used in place of the coordinate value and the optimization was allowed to proceed. This approach allowed optimizations to continue even when the BFGS optimizer was exploring unphysical basis set parameter values. This problem was predominantly present in early optimization cycles,

Table 2. Optimized Atomic Parameter Values for the PM6 Basis Set for Ru

parameter	value	parameter	value	parameter	value
$U_{ss}$ [ $E_h$ ]	-1.7604831845	F0ss	0.106882438247	DDN 0,1	0.0973693655176
$U_{pp}$ [ $E_h$ ]	-1.40929763024	F0sp	0.26555585717	DDN 1,1	0.461423790056
$U_{dd}$ [ $E_h$ ]	-1.43820061041	F0pp	0.769040859112	DDN 0,2	1.24169378781
$\beta_s$ [ $E_h^{-1}$ ]	-0.485079071544	F0sd	0.239150007906	DDN 1,2	0.291020714169
$\beta'_s$ [ $E_h^{-1}$ ]	-0.279166913525	F0pd	0.174441468209	DDN 2,2	0.857452893985
$\beta_s$ [ $E_h^{-1}$ ]	-0.0845524891951	F0dd	0.15960281913	coreKO	3.15044514551
$\zeta'_s$ [ $a_0^{-1}$ ]	1.61139618742	F2pp	0.447902498139	KON 0,0,0	3.08598108139
$\zeta_p$ [ $a_0^{-1}$ ]	5.54753977766	F2pd	0.0578471433046	KON 1,0,1	1.53385840269
$\zeta_d$ [ $a_0^{-1}$ ]	1.96471657601	F2dd	0.0467229771373	KON 0,1,1	3.06678130426
$z_{sn}$ [ $a_0^{-1}$ ]	0.984449	F4dd	0.150889145233	KON 2,1,1	0.432919457955
$z_{pn}$ [ $a_0^{-1}$ ]	4.586613	G1sp	-0.0187261503385	KON 2,0,2	0.874832538452
$z_{dn}$ [ $a_0^{-1}$ ]	0.765332	G1pd	0.00292795157994	KON 1,1,2	2.93437053908
		G2sd	0.194244551364	KON 0,2,2	3.16492704166
		G3pd	0.0180183403523	KON 2,2,2	1.36213361378
		rsppd	-0.0323190566131	EHeat	0.2478050256
		rsdpp	0.062983642067	dipHyp	0.1850948538
		rsddd	0.103038833118		

diminishing or disappearing in later cycles when the parameter set was closer to an optimized value.

All calculations were carried out using the Gaussian 09<sup>4</sup> computational chemistry package.<sup>57</sup> Calculations were made using the semiempirical PM6 method in vacuum.<sup>36</sup> As this method is relatively inexpensive to evaluate, the optimizations proceeded rather quickly. The code to conduct the optimization was written in Python and used the BFGS optimizer from the SciPy package.<sup>58,59</sup> The code was written to perform Gaussian calculations in parallel to improve efficiency on a multicore computer. The default basis set parameters for the PM6 method were used as initial parameters for all optimization runs. Optimizations were typically completed after a significant reduction in the objective function value, but before an optimization convergence criterion was reached. This happened because the objective function became increasingly insensitive to changes in the parameters as its value decreased.

## RESULTS AND DISCUSSION

**Optimization of PM6 Basis Set Parameters.** Optimization of the basis set parameters for Ru was performed in the manner described above. Weight factors were assigned for each molecule in the fitting set such that errors in bond lengths ( $\text{\AA}$ ) were weighted 10 times more than errors in bond angles (deg). This was done to minimize the error due to bond lengths since the error in bond angles was already small and considered acceptable and because correcting small errors in geometry can yield a noticeable improvement in the electronic structure. In most runs (and in the final results), only the basis set for Ru was optimized. It was found that optimizing additional basis sets (e.g., those for H, C, N, O, and S) did not improve the results significantly. The optimization was completed in 17 steps, requiring 85 function and 75 gradient evaluations. Over the course of the optimizations, the value of the objective function decreased by a factor of 4. The optimization was terminated when it was determined that further adjustment of the parameters was not reducing the value of the objective function.

Optimized basis set parameters for the Ru atom using the PM6 Hamiltonian produced using the procedure described in the previous section are presented in Table 2 (atomic parameters) and Table 3 (diatomic parameters). In some

Table 3. Optimized Diatomic Parameter Values for the PM6 Basis Set for Ru

bond	$\alpha_{ij}$ [ $a_0^{-1}$ ]	$x_{ij}$
Ru-H	1.46613642493	7.13944272757
Ru-C	1.50787067227	1.13012940396
Ru-N	1.66244074163	2.40223510806
Ru-O	1.6589387983	2.976279
Ru-S	1.3272166566	1.006683

cases, the parameter values change very little from the default PM6 basis set, while other parameters changed significantly. Typically, the optimized parameters varied from the default PM6 basis set parameters by 10% or less. Larger changes were observed in the *F*, *G*, and *R* parameters.

**Evaluation of PM6 Optimizations.** Optimized geometries were found using the PM6 method with the default basis set parameters for Ru (and all other atoms) for each molecule in the full set of 20 molecules. The overall mean unsigned error of these results versus the optimized DFT geometries is 0.0433  $\text{\AA}$  for bond lengths and 0.96° for bond angles over the set of inner-sphere coordinates examined (see above and Supporting Information for full details of which coordinates were used). The results show a range of deviations, from a minimum of 0.0165  $\text{\AA}$  to a maximum of 0.1009  $\text{\AA}$  in bond lengths, with errors of ca. 0.05  $\text{\AA}$  being common. Deviations in bond angle are typically around 1°, but span a range of 0.13°–3.08°. The PM6 basis set produces geometries whose average error is within the tolerance expected for computational results for these types of transition metal complexes. However, it seems to treat all Ru-N and Ru-C bonds the same regardless of the ligand and bonding group, i.e., 8-quinolines vs pyridines or cyclomethylated vs carbene ligands.

To improve the optimized structures, find better matches to optimized DFT structure, and therefore represent the bonding chemistry more accurately, we reparametrized the PM6 Ru basis set. When the optimized basis set parameters for Ru developed in this work are used with the PM6 method, the mean unsigned error versus the DFT values is 0.0170  $\text{\AA}$  in bond lengths and 0.91° in bond angles for the set of coordinates examined. Deviations in bond lengths range from 0.0026 to 0.0737  $\text{\AA}$ , with typical values around 0.01–0.02  $\text{\AA}$ . Bond angle

deviations range from 0.19° to 2.72°, with typical values less than 1°. From the results in Table 4 it can be seen that the

**Table 4. Mean Unsigned Error (MUE) in Bond Length (Å) and Bond Angle (deg) for 20 DSC Molecules Optimized Using Default and Optimized PM6 Parameters Compared to Optimized DFT Structures**

molecule	default parameters		optimized parameters	
	MUE (bond, Å)	MUE (angle, deg)	MUE (bond, Å)	MUE (angle, deg)
Ru(NCN) <sub>2</sub>	0.0309	1.47	0.0250	2.08
Ru(DNinP) <sub>2</sub>	0.0427	1.01	0.0071	0.33
Ru(DQB) <sub>2</sub>	0.0165	0.23	0.0180	0.66
Ru(DQIm) <sub>2</sub>	0.0267	0.36	0.0117	0.63
Ru(DQPCOOH) <sub>2</sub>	0.0479	0.85	0.0084	0.27
Ru(DQPFur) <sub>2</sub>	0.1009	3.08	0.0737	2.72
Ru(DQPNH <sub>2</sub> ) <sub>2</sub>	0.0532	0.93	0.0126	0.20
Ru(DQP1) <sub>2</sub>	0.0436	1.86	0.0287	1.45
Ru(DQPz) <sub>2</sub>	0.0519	1.14	0.0118	0.51
N <sub>3</sub>	0.0176	1.18	0.0200	1.05
Ru(PzPyPz) <sub>2</sub>	0.0544	0.23	0.0077	1.19
Ru(PzbPybPz) <sub>2</sub>	0.0305	0.13	0.0157	0.48
Ru(CPyC)(TPy)	0.0226	0.88	0.0146	1.58
black	0.0400	0.36	0.0120	0.37
Ru(BPy) <sub>3</sub>	0.0437	1.08	0.0026	0.72
Ru(DQP) <sub>2</sub>	0.0458	0.91	0.0058	0.19
Ru(DBPzP) <sub>2</sub>	0.0514	1.79	0.0334	1.28
Ru(DQxP) <sub>2</sub>	0.0552	0.17	0.0121	1.01
Ru(DCpP) <sub>2</sub>	0.0546	1.23	0.0131	0.98
Ru(TPy) <sub>2</sub>	0.0366	0.33	0.0057	0.56
overall	0.0433	0.96	0.0170	0.91

optimized PM6 basis set for Ru improves agreement with the optimized DFT geometries, particularly for bond lengths (a factor of 2.5 improvement), while the performance for bond angles is essentially the same. This is not surprising as the optimization was biased toward minimization of bond length errors. The  $\approx 2.5\times$  reduction in bond distance error with the optimized parameter set is important since it improves the agreement between PM6 calculated structures and known crystal structures and because the improved bond lengths have a significant effect on the UV/vis spectra.

The training set includes a range of Ru–N bonding including pyridine, pyrazole, quinoline, and thiocyno motifs. However, the optimized parameters based on this set improved agreement with Ru–C bond distances and with imidazole, pyrrole, and bridging motifs as well. While these results show that significant improvement can be obtained by generating specific parameters for a family of molecules, the performance of the default PM6 basis set for Ru is nevertheless commendable.

**Practical Implications.** Since we have demonstrated that PM6 with either set of basis set parameters yields optimized geometries for Ru(II) compounds in good agreement with optimized DFT geometries, we now discuss practical uses for PM6 in studying DSC compounds. We first examine the usefulness of PM6-optimized geometries as starting geometries for DFT optimizations.

To test the PM6 method for preliminary optimization of DSC compounds, we optimized three representative structures with the default PM6 basis set parameters, with our optimized

PM6 basis set parameters, and with DFT (PBE0/6-31G(d,p)-[C,N,H]/SDD[Ru]/PCM(CH<sub>3</sub>CN)). Each of the optimizations was started from a molecular mechanics method (MM2) optimized geometry of the complex, representing the kind of “flat ligand” structures where the ligands are obtained from a 2D representation or chemical drawing. Structures created in this manner are appropriate in a screening context where many candidate structures may be automatically generated and tested.

The efficacy of the starting structure is judged by the number of steps the subsequent DFT optimization takes to reach a minimum energy geometry. The number of optimization steps required (Table 5) for each of the three structures varied from

**Table 5. Representative Number of Optimization Steps and Average Self-Consistent Field Cycles (Denoted SCF) Needed To Converge Each Structure Using All Optimization Methods<sup>a</sup>**

optimization method	Ru(DQP) <sub>2</sub>		Ru(TPy) <sub>2</sub>		Ru(DBPzP) <sub>2</sub>	
	steps	SCF	steps	SCF	steps	SCF
default PM6	47	19.2	13	16.7	233	289.0
optimized PM6	50	19.1	12	15.8	61	25.1
DFT	70	13.6	13	11.3	90	18.8
default PM6 + DFT	8	11.0	4	12.0	80	18.4
optimized PM6 + DFT	8	10.9	4	11.5	77	15.2

<sup>a</sup>DFT is PBE0/6-31G(d,p)-[C,N,O,S,H]SDD[Ru]/PCM(CH<sub>3</sub>CN).

12 steps to 233 steps across PM6 and DFT methods. The Ru(TPy)<sub>2</sub> optimized geometry has planar ligands whose bond lengths are dominated by steric effects. In contrast, while the ligands of Ru(DBPzP)<sub>2</sub> are also planar, the bond distances, especially around the Ru center, are dominated by electronic effects. Finally, Ru(DQP)<sub>2</sub> has a significant ligand backbone twist. The steps needed to optimize each of these depends on both how different the minimum is from the starting geometry and the geometric or electronic effects that influence the final minimum.

By starting with an optimized geometry computed using PM6, the number of DFT steps required to find a minimum was reduced from 70 to 8 for Ru(DQP)<sub>2</sub> and from 13 to 4 for Ru(TPy)<sub>2</sub>. For Ru(DBPzP)<sub>2</sub>, whose interactions depend less on structural factors and instead are driven by electronic factors, 77 DFT optimization steps were needed to converge, providing only a modest improvement. The discrepancy in the number of DFT optimization steps noted above may be explained by noting that the preoptimized structure for Ru(DBPzP)<sub>2</sub> is significantly “farther” from the minimum energy structure than that of Ru(DQP)<sub>2</sub> or Ru(TPy)<sub>2</sub> (Table 6). The performance of the optimized basis set parameters versus the default basis set parameters was identical for the first two compounds and was slightly better for the final compound when using the optimized structures produced using these basis sets to start DFT optimizations.

While the numbers of steps to achieve a final DFT optimized structure are similar for the two PM6 methods, the optimized PM6 method provides consistently lower energy structures versus the default parameters, which range from  $\approx 60$  to  $\approx 180$  kJ mol<sup>-1</sup> higher, even though energetics were not considered in the basis set reparametrization. While the geometries are very similar, each of the optimized PM6 structures is still at least 35 kJ mol<sup>-1</sup> higher in energy than the optimized DFT minima. In contrast, all of the DFT optimized structures were found to have identical geometries within the convergence tolerance.

**Table 6. Relative Energies of Three Representatively Optimized Structures Starting from MM2 Optimized 2D Structures Using All Methods<sup>a</sup>**

optimization method	Ru(DQP) <sub>2</sub>	Ru(TPy) <sub>2</sub>	Ru(DBPzP) <sub>2</sub>
default PM6	144.33	178.01	58.92
optimized PM6	0.0	0.0	0.0
DFT/optimized PM6	46.50	35.57	136.24
DFT	0.0002	0.005	0.007
default PM6+DFT	0.0001	0.0	0.0
optimized PM6+DFT	0.0	0.0008	0.40

<sup>a</sup>Energies are relative to the lowest energy of either DFT or PM6 optimized and are in kJ mol<sup>-1</sup>, and DFT is PBE0/6-31G(d,p)-[C,N,O,S,H]SDD[Ru]/PCM(CH<sub>3</sub>CN).

In general, it is clear that preoptimization using PM6 with either the default basis set or the optimized basis set presented in this work can significantly reduce the amount of computer time required to find a DFT optimized structure. The simple reason for this is that a full optimization with PM6 will take much less time than one DFT optimization cycle for the molecules considered here. Thus, PM6 preoptimization is recommended for studies in which optimized structures of DSC molecules are desired. This is not a surprising result, as it has long been known that the use of a lower level method or a smaller basis set (or both) can produce good results in a fraction of the time otherwise required. Nevertheless, this work validates the use of PM6 for this purpose for DSC compounds. Furthermore, when an initial structure needs to be refined, the use of the PM6 method can significantly reduce the time required to achieve acceptable results. This is not only useful in its own right but also suggests that PM6 calculations may be useful for screening large numbers of candidate structures. Screening sets of structures requires evaluating the critical physics and chemistry of a complex in a cost-effective manner.

As these chromophores are excited by light, the alignment of the excited states is critical to their performance. TD-DFT often reproduces the absorption spectra of Ru dyes quite well at this level of theory when using a PCM solvent.<sup>26,56</sup> However, calculating excited states is always more computationally expensive and needs to be done more carefully. Ru parameters for the semiempirical alternative ZINDO method are not readily available in most quantum codes. Thus, a common method used to evaluate Ru-based dyes for DSCs, explored by De Angelis and Fantacci,<sup>60</sup> has been to compare the highest occupied molecular orbital (HOMO) to the lowest unoccupied molecular orbital (LUMO) gaps of molecular candidates. This relies on the assumption that electrons are injected from an

excited state that is well described as a simple HOMO–LUMO excitation, which is true for most Ru(II) complexes where the HOMO is composed of Ru *d* orbitals and the LUMOs are ligand centered, leading to the common MLCT (singlet and triplet) excitations. This description of the electronic structure and UV/vis spectrum are both highly dependent on the underlying ground state structure.

The main interaction where improvement over PM6 is most noticeable in these complexes is in shortening the Ru–N and Ru–C bonds when the binding group strongly donates electron density to the Ru center. PM6 treats all Ru–N (and Ru–C) bonds as equivalent, leading to slightly unrealistic inner-sphere coordination structure. In particular, strongly electron-donating equatorial groups on tridentate ligands (e.g., the Ru–quinoline bonds in Ru(DQP)<sub>2</sub>) are known to increase the stability of the light harvester during excitation, since the strong Ru–ligand bonds reduce the risk of ligand loss.<sup>20,51</sup> These stronger Ru–ligand bonds are shorter in the crystal structures of such complexes (Table 7) forcing the axial (or center) ring–Ru bond to also be shorter due to ligand sterics. PBE0/6-31G(d,p)[C,N,H]/SDD[Ru]/PCM(CH<sub>3</sub>CN) is known to reproduce experimental crystal structures well by accurately predicting the different lengths of inner-sphere Ru–N or Ru–C bonds. PM6 without the optimized Ru basis set overestimates these bond lengths (Table 7). In complexes like Ru(TPy)<sub>2</sub>, where equatorial and axial groups are equivalent, optimization of the PM6 parameters reduces these bond lengths, bringing them closer to those found by DFT. In systems like Ru(DQP)<sub>2</sub>, however, the optimized PM6 parameters not only improve agreement with DFT but also predict the differences in equatorial and axial bond lengths (Table 7).

Studying the electronic structure using HOMO–LUMO gaps, we examined the differences between PM6 methods and the DFT optimized structure. The shifts in molecular orbital energies are larger (Figure S1) and the HOMO–LUMO gaps smaller (Table S1) for the DFT optimized structures than for the optimized PM6 structures, as it is well-known that DFT tends to underestimate HOMO–LUMO gaps. While the magnitudes of energies and energy levels, octahedrality, and HOMO–LUMO gaps in the two sets of optimized structures differs, good structural matches achieved with the optimized PM6 method mean that the overall trends are consistent with the DFT results (Figure 1).

Small changes in geometry produced by the optimized PM6 parameters have a significant effect on the UV/vis spectra. This is illustrated by calculating TD-DFT spectra from each of the DFT, PM6, and optimized PM6 relaxed geometries (Figure 2)

**Table 7. Comparison of Ru–N Bond Lengths and Octahedrality between Experiment and Computation**

complex	geometry	R <sup>a</sup> (Å)	R <sub>e</sub> <sup>b</sup> (Å)	R <sub>a</sub> <sup>c</sup> (Å)	O <sup>d</sup> (deg)
Ru(DQP) <sub>2</sub>	experimental	2.07 ± 0.04	2.09 ± 0.04	2.04 ± 0.03	1.27
	default PM6	2.12 ± 0.003	2.13 ± 0.001	2.11 ± 0.0004	1.42
	optimized PM6	2.08 ± 0.003	2.09 ± 0.0009	2.07 ± 0.0002	1.13
	DFT	2.08 ± 0.01	2.09 ± 0.00	2.05 ± 0.0001	0.89
Ru(TPy) <sub>2</sub>	experimental	2.04 ± 0.04	2.07 ± 0.01	1.99 ± 0.00	8.83
	default PM6	2.09 ± 0.02	2.13 ± 0.00	2.01 ± 0.00	8.42
	optimized PM6	2.05 ± 0.02	2.09 ± 0.00	1.98 ± 0.00	7.51
	DFT	2.05 ± 0.02	2.09 ± 0.00	1.99 ± 0.00	8.15

<sup>a</sup>Overall average bond length. <sup>b</sup>Average equatorial bond length, where the equatorial bond distance is measured from the Ru to the quinoline groups for Ru(DQP)<sub>2</sub>. <sup>c</sup>Average axial bond length. <sup>d</sup>Octahedrality, i.e., the deviation of angles from a perfect octahedron, calculated as the root-mean-square of the angles from an ideal octahedron, 90°.

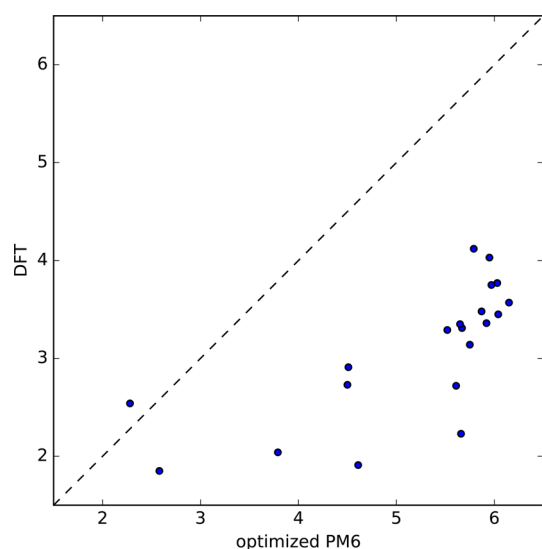


**Figure 1.** Correlation of DFT, PBE0/6-31G(d,p)[C,N,O,S,H]SDD[Ru]/PCM(CH<sub>3</sub>CN), versus optimized PM6 HOMO–LUMO gaps (eV).

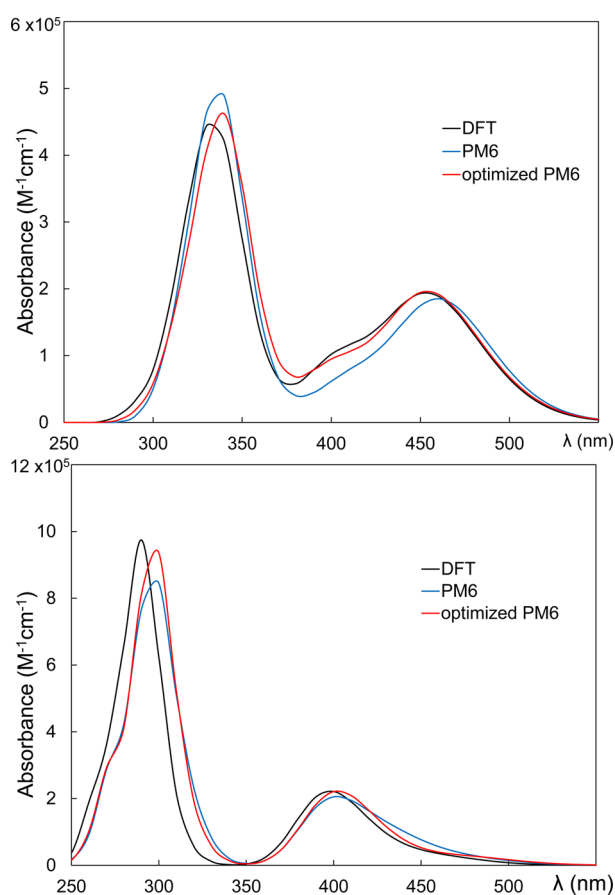


**Figure 2.** Calculated absorption spectra of relaxed DFT, PM6, and optimized PM6 geometries for Ru(DQP)<sub>2</sub> (top) and Ru(TPy)<sub>2</sub> (bottom). Spectra are 0.2 eV broadened TD-DFT using PBE0/6-31G(d,p)[C,N,O,S,H]SDD[Ru]/PCM(CH<sub>3</sub>CN).

and shows that the optimized PM6 structures provide a closer match to the spectra computed from the DFT structures. In particular, for Ru(DQP)<sub>2</sub>, the excitations from the PM6 geometry are missing a distinct MLCT shoulder at  $\approx 400$  nm.

In the DFT results, this is a Ru– $t_{2g}$  to quinoline– $\pi^*$  excitation. In the PM6 spectrum, the longer Ru–quinoline bonds reduce the intensity of this transition, shifting it to longer wavelengths and making it merely broaden the stronger MLCT peak at  $\approx 450$  nm seen in the TD-DFT spectra of all of the structures. The shorter Ru–quinoline bonds in the optimized PM6 correctly recover this shoulder. Clearly, the small changes in inner-sphere Ru–N and Ru–C bond lengths make a noticeable difference in the UV/vis spectra.

## CONCLUSION

In this article, the use of semiempirical methods for studying the structures of transition metal centered molecules is studied. In particular, Ru-containing dye-sensitized solar cell chromophore molecules were considered. The semiempirical PM6 Hamiltonian provides reasonable structural matches to well-optimized DFT structures at the PBE0/6-31G(d,p)-SDD/PCM level of theory. In order to improve the agreement between the PM6 and PBE0 results, the default PM6 basis set for Ru was optimized using a set of six Ru-containing molecules. Testing was done using a set of 20 molecules that included the six molecules used in training. Optimization of the PM6 basis set for Ru improves agreement with the PBE0 optimized structures with a reduction in the mean unsigned error in bond lengths from 0.0433 Å using the default basis set to 0.0170 Å using the optimized basis set. The mean unsigned error in bond angles was reduced from 0.96° to 0.91°. The results of this study suggest that further improvement in the agreement with the PBE0 results will be difficult to obtain without a change to the PM6 Hamiltonian itself. Nevertheless, these relatively small geometric changes are important in correctly capturing features of the electronic structure and thus the UV/vis spectrum.

Geometry optimization of large metal centered compounds can be a time-consuming process. The results of the present study indicate that the semiempirical PM6 method, particularly using an optimized basis set such as that presented here, is valuable for refining candidate structures and for generating high-quality initial structures for further geometric optimization using more expensive quantum chemistry methods. Generally good agreement for geometry and electronic structure indicates that the PM6 method, particularly with the optimized basis set parameters developed in this article, will be of considerable use in rapidly screening a large number of candidate molecules for use in dye-sensitized solar cell applications.

## ASSOCIATED CONTENT

### Supporting Information

The Supporting Information is available free of charge on the ACS Publications website at DOI: 10.1021/acs.jpca.6b00921.

HOMO–LUMO gaps, Ru basis set in Gaussian format, Cartesian coordinates of optimized structures, and TD-DFT transitions (PDF)

## AUTHOR INFORMATION

### Corresponding Author

\*E-mail: [lisa.fredin@nist.gov](mailto:lisa.fredin@nist.gov) (L.A.F.).

### Notes

The authors declare no competing financial interest.

## ACKNOWLEDGMENTS

L.A.F. acknowledges funding from the NIST-NRC fellowship program.

## ■ ADDITIONAL NOTE

<sup>a</sup>Certain commercial equipment, instruments, or materials are identified in this paper in order to specify the experimental procedure adequately. Such identification is not intended to imply recommendation or endorsement by the National Institute of Standards and Technology, nor is it intended to imply that the materials or equipment identified are necessarily the best available for the purpose.

## ■ REFERENCES

- (1) Lewis, N. S.; Nocera, D. G. Powering the Planet: Chemical Challenges in Solar Energy Utilization. *Proc. Natl. Acad. Sci. U. S. A.* **2006**, *103*, 15729–15735.
- (2) Graetzel, M.; Janssen, R. A. J.; Mitzi, D. B.; Sargent, E. H. Materials Interface Engineering for Solution-Processed Photovoltaics. *Nature* **2012**, *488*, 304–312.
- (3) Nazeeruddin, M. K.; Kay, A.; Rodicio, I.; Humphry-Baker, R.; Mueller, E.; Liska, P.; Vlachopoulos, N.; Graetzel, M. Conversion of Light to Electricity by *cis*-X<sub>2</sub>Bis(2,2'-bipyridyl-4,4'-dicarboxylate)-ruthenium(II) Charge-Transfer Sensitizers (X = Cl<sup>-</sup>, Br<sup>-</sup>, I<sup>-</sup>, CN<sup>-</sup>, and SCN<sup>-</sup>) on Nanocrystalline Titanium Dioxide Electrodes. *J. Am. Chem. Soc.* **1993**, *115*, 6382–6390.
- (4) Gust, D.; Moore, T. A.; Moore, A. L. Solar Fuels Via Artificial Photosynthesis. *Acc. Chem. Res.* **2009**, *42*, 1890–1898.
- (5) Sauvage, J. P.; Collin, J. P.; Chambron, J. C.; Guillerez, S.; Coudret, C.; Balzani, V.; Barigelli, F.; De Cola, L.; Flamigni, L. Ruthenium(II) and Osmium(II) Bis(terpyridine) Complexes in Covalently-Linked Multicomponent Systems: Synthesis, Electrochemical Behavior, Absorption Spectra, and Photochemical and Photophysical Properties. *Chem. Rev.* **1994**, *94*, 993–1019.
- (6) Friedman, A. E.; Chambron, J. C.; Sauvage, J. P.; Turro, N. J.; Barton, J. K. A Molecular Light Switch for DNA: Ru(bpy)<sub>2</sub>(dppz)<sup>2+</sup>. *J. Am. Chem. Soc.* **1990**, *112*, 4960–4962.
- (7) Ardo, S.; Meyer, G. J. Photodriven Heterogeneous Charge Transfer with Transition-Metal Compounds Anchored to TiO<sub>2</sub> Semiconductor Surfaces. *Chem. Soc. Rev.* **2009**, *38*, 115–164.
- (8) Barigelli, F.; Flamigni, L. Photoactive Molecular Wires Based on Metal Complexes. *Chem. Soc. Rev.* **2000**, *29*, 1–12.
- (9) Alstrum-Acevedo, J. H.; Brennaman, M. K.; Meyer, T. J. Chemical Approaches to Artificial Photosynthesis. 2. *Inorg. Chem.* **2005**, *44*, 6802–6827.
- (10) Juris, A.; Balzani, V.; Barigelli, F.; Campagna, S.; Belser, P.; von Zelewsky, A. Ru(II) Polypyridine Complexes: Photophysics, Photochemistry, Electrochemistry, and Chemiluminescence. *Coord. Chem. Rev.* **1988**, *84*, 85–277.
- (11) Calvert, J. M.; Caspar, J. V.; Binstead, R. A.; Westmoreland, T. D.; Meyer, T. J. Metallopolymer Photochemistry. Photophysical, Photochemical and Photoelectrochemical Properties of (bpy)<sub>2</sub>Ru<sup>II</sup> Sites Bound to Poly(4-vinylpyridine). *J. Am. Chem. Soc.* **1982**, *104*, 6620–6627.
- (12) Winkler, J. R.; Netzel, T. L.; Creutz, C.; Sutin, N. Direct Observation of Metal-To-Ligand Charge-Transfer (MLCT) Excited States of Pentaammineruthenium(II) Complexes. *J. Am. Chem. Soc.* **1987**, *109*, 2381–2392.
- (13) Lever, A. B. P. Electrochemical Parametrization of Metal Complex Redox Potentials, Using the Ruthenium(III)/Ruthenium(II) Couple to Generate a Ligand Electrochemical Series. *Inorg. Chem.* **1990**, *29*, 1271–1285.
- (14) Elliott, C. M.; Hershenhart, E. J. Electrochemical and Spectral Investigations of Ring-Substituted Bipyridine Complexes of Ruthenium. *J. Am. Chem. Soc.* **1982**, *104*, 7519–7526.
- (15) Maestri, M.; Armaroli, N.; Balzani, V.; Constable, E. C.; Cargill Thompson, A. M. W. Complexes of the Ruthenium(II)-2,2'/6',2''-Terpyridine Family - Effect of Electron-Accepting and Electron-Donating Substituents on the Photophysical and Electrochemical Properties. *Inorg. Chem.* **1995**, *34*, 2759–2767.
- (16) Duati, M.; Tasca, S.; Lynch, F. C.; Bohlen, H.; Vos, J. G.; Stagni, S.; Ward, M. D. Enhancement of Luminescence Lifetimes of

Mononuclear Ruthenium(II)-Terpyridine Complexes by Manipulation of the  $\sigma$ -Donor Strength of Ligands. *Inorg. Chem.* **2003**, *42*, 8377–8384.

(17) Abbotto, A.; Manfredi, N. Electron-Rich Heteroaromatic Conjugated Polypyridine Ruthenium Sensitizers for Dye-Sensitized Solar Cells. *Dalton Trans.* **2011**, *40*, 12421–12438.

(18) Abrahamsson, M.; Hedberg, J. H. J.; Becker, H.-C.; Staniszewski, A.; Pearson, W. H.; Heuer, W. B.; Meyer, G. J. High Extinction Coefficient Ru-Sensitizers That Promote Hole Transfer on Nanocrystalline TiO<sub>2</sub>. *ChemPhysChem* **2014**, *15*, 1154–1163.

(19) Wang, Y.; Liu, S.; Pinto, M. R.; Dattelbaum, D. M.; Schoonover, J. R.; Schanze, K. S. Excited-State Structure and Delocalization in Ruthenium(II)Bipyridine Complexes That Contain Phenyleneethynylene Substituents. *J. Phys. Chem. A* **2001**, *105*, 11118–11127.

(20) Brown, D. G.; Sanguantrakun, N.; Schulze, B.; Schubert, U. S.; Berlinguette, C. P. Bis(tridentate) Ruthenium-Terpyridine Complexes Featuring Microsecond Excited-State Lifetimes. *J. Am. Chem. Soc.* **2012**, *134*, 12354–12357.

(21) Williams, J. A. G. the Coordination Chemistry of Dipyr- idylbenzene: N-Deficient Terpyridine or Panacea for Brightly Luminescent Metal Complexes? *Chem. Soc. Rev.* **2009**, *38*, 1783–1801.

(22) Abrahamsson, M.; Becker, H. C.; Hammarström, L.; Bonnefous, C.; Chamchoum, C.; Thummel, R. P. Six-Membered Ring Chelate Complexes of Ru(II): Structural and Photophysical Effects. *Inorg. Chem.* **2007**, *46*, 10354–10364.

(23) Abrahamsson, M.; Jäger, M.; Österman, T.; Eriksson, L.; Persson, P.; Becker, H.-C.; Johansson, O.; Hammarström, L. A 3.0  $\mu$ s Room Temperature Excited State Lifetime of a Bistridentate Ru<sup>II</sup>-Polypyridine Complex for Rod-like Molecular Arrays. *J. Am. Chem. Soc.* **2006**, *128*, 12616–12617.

(24) Liu, Y.; Harlang, T.; Canton, S. E.; Chábera, P.; Suárez-Alcántara, K.; Fleckhaus, A.; Vithanage, D. A.; Göransson, E.; Corani, A.; Lomoth, R.; et al. Towards Longer-Lived Metal-to-Ligand Charge Transfer States of Iron(II) Complexes: An N-Heterocyclic Carbene Approach. *Chem. Commun.* **2013**, *49*, 6412–6414.

(25) Liu, Y.; Kjaer, K. S.; Fredin, L. A.; Chábera, P.; Harlang, T.; Canton, S. E.; Lidin, S.; Zhang, J.; Lomoth, R.; Bergquist, K.-E.; et al. A Heteroleptic Ferrous Complex with Mesoionic bis(1,2,3-triazol-5-ylidene) Ligands: Taming the MLCT Excited State of Iron(II). *Chem. - Eur. J.* **2015**, *21*, 3628–3639.

(26) Parada, G. A.; Fredin, L. A.; Santoni, M. P.; Jäger, M.; Lomoth, R.; Hammarström, L.; Johansson, O.; Persson, P.; Ott, S. Tuning the Electronics of Bis(tridentate)ruthenium(II) Complexes with Long-Lived Excited States: Modifications to the Ligand Skeleton Beyond Classical Electron Donor or Electron Withdrawing Group Decorations. *Inorg. Chem.* **2013**, *52*, 5128–5137.

(27) Jarenmark, M.; Fredin, L. A.; Hedberg, J. H. J.; Doverbratt, I.; Persson, P.; Abrahamsson, M. A Homoleptic Trisbidentate Ru(II) Complex of a Novel Bidentate Biheteroaromatic Ligand Based on Quinoline and Pyrazole Groups: Structural, Electrochemical, Photo-physical, and Computational Characterization. *Inorg. Chem.* **2014**, *53*, 12778–12790.

(28) Vlček, A., Jr. The Life and Times of Excited States of Organometallic and Coordination Compounds. *Coord. Chem. Rev.* **2000**, *200–202*, 933–978.

(29) Vlček, A., Jr.; Zálivs, S. Modeling of Charge-Transfer Transitions and Excited States in d<sup>6</sup> Transition Metal Complexes by DFT Techniques. *Coord. Chem. Rev.* **2007**, *251*, 258–287.

(30) Cramer, C. J.; Truhlar, D. G. Density Functional Theory for Transition Metals and Transition Metal Chemistry. *Phys. Chem. Chem. Phys.* **2009**, *11*, 10757–10816.

(31) Fantacci, S.; De Angelis, F. A Computational Approach to the Electronic and Optical Properties of Ru(II) and Ir(III) Polypyridyl Complexes: Applications to DSC, OLED and NLO. *Coord. Chem. Rev.* **2011**, *255*, 2704–2726.

(32) Österman, T.; Abrahamsson, M.; Becker, H.-C.; Hammarström, L.; Persson, P. Influence of Triplet State Multidimensionality on Excited State Lifetimes of Bis-Tridentate RuII Complexes: A Computational Study. *J. Phys. Chem. A* **2012**, *116*, 1041–1050.

- (33) Fredin, L. A.; Pápai, M.; Rozsályi, E.; Vankó, G.; Wärnmark, K.; Sundström, V.; Persson, P. Exceptional Excited-State Lifetime of an Iron(II)-N-Heterocyclic Carbene Complex Explained. *J. Phys. Chem. Lett.* **2014**, *5*, 2066–2071.
- (34) Dewar, M. J. S.; Zebisch, E. G.; Healy, E. F.; Stewart, J. J. P. Development and Use of Quantum Mechanical Molecular Models. 76. AM1: A New General Purpose Quantum Mechanical Molecular Model. *J. Am. Chem. Soc.* **1985**, *107*, 3902.
- (35) Stewart, J. J. P. Optimization of Parameters for Semiempirical Methods I. Method. *J. Comput. Chem.* **1989**, *10*, 209–220.
- (36) Stewart, J. J. P. Optimization of Parameters for Semiempirical Methods V: Modification of NDDO Approximations and Application to 70 Elements. *J. Mol. Model.* **2007**, *13*, 1173–1213.
- (37) Stewart, J. J. P. Optimization of Parameters for Semiempirical Methods VI: More Modifications to the NDDO Approximations and Re-Optimization of Parameters. *J. Mol. Model.* **2013**, *19*, 1–32.
- (38) Rillema, D. P.; Jones, D. S.; Woods, C.; Levy, H. A. Comparison of the Crystal Structures of Tris Heterocyclic Ligand Complexes of Ruthenium(II). *Inorg. Chem.* **1992**, *31*, 2935–2938.
- (39) Eskelinen, E.; Luukkanen, S.; Haukka, M.; Ahlgren, M.; Pakkanen, T. A. Redox and Photochemical Behaviour of Ruthenium(II) Complexes with H<sub>2</sub>dcbpy Ligand (H<sub>2</sub>dcbpy = 2,2'-bipyridine-4,4'-dicarboxylic Acid). *J. Chem. Soc., Dalton Trans.* **2000**, 2745–2752.
- (40) Péchy, P.; Renouard, T.; Zakeeruddin, S. M.; Humphry-Baker, R.; Comte, P.; Liska, P.; Cevey, L.; Costa, E.; Shklover, V.; Spiccia, L.; et al. Engineering of Efficient Panchromatic Sensitizers for Nanocrystalline TiO<sub>2</sub>-Based Solar Cells. *J. Am. Chem. Soc.* **2001**, *123*, 1613–1624.
- (41) Pyo, S.; Pérez-Cordero, E.; Bott, S. G.; Echegoyen, L. Crystal Structure of [Ru(terpy)<sub>2</sub>]<sup>0</sup>: A New Crystalline Material from the Reductive Electrocrystallization of [Ru(terpy)<sub>2</sub>]<sup>2+</sup>. *Inorg. Chem.* **1999**, *38*, 3337–3343.
- (42) Jameson, D. L.; Blaho, J. K.; Kruger, K. T.; Goldsby, K. A. Redox Regulation in Ruthenium(II) Complexes of 2,6-bis(N-pyrazolyl)pyridine Ligands: Synthetically Versatile Analogs of 2,2':6',2''-terpyridine. *Inorg. Chem.* **1989**, *28*, 4312–4314.
- (43) Bhaumik, C.; Das, S.; Saha, D.; Dutta, S.; Baitalik, S. Synthesis, Characterization, Photophysical, and Anion-Binding Studies of Luminescent Heteroleptic Bis-tridentate Ruthenium(II) Complexes Based on 2,6-bis(benzimidazole-2-yl)pyridine and 4'-Substituted 2,2':6',2''-terpyridine Derivatives. *Inorg. Chem.* **2010**, *49*, 5049–5062.
- (44) Abrahamsson, M.; Jäger, M.; Kumar, R. J.; Österman, T.; Persson, P.; Becker, H.-C.; Johansson, O.; Hammarström, L. Bistridentate Ruthenium(II)polypyridyl-Type Complexes with Microsecond <sup>3</sup>MLCT State Lifetimes: Sensitizers for Rod-like Molecular Arrays. *J. Am. Chem. Soc.* **2008**, *130*, 15533–15542.
- (45) Laemmel, A.-C.; Collin, J.-P.; Sauvage, J.-P. Photosubstitution of Ancillary Ligands in Octahedral Mono-Terpyridine Ruthenium(II) Complexes. *C. R. Acad. Sci., Ser. IIC: Chim.* **2000**, *3*, 43–49.
- (46) Schramm, F.; Meded, V.; Fliegl, H.; Fink, K.; Fuhr, O.; Qu, Z.; Klopfer, W.; Finn, S.; Keyes, T. E.; Ruben, M. Expanding the Coordination Cage: A Ruthenium(II)-Polypyridine Complex Exhibiting High Quantum Yields Under Ambient Conditions. *Inorg. Chem.* **2009**, *48*, 5677–5684.
- (47) Jarenmark, M.; Carlström, G.; Fredin, L. A.; Wallenstein, J. H.; Doverbratt, I.; Abrahamsson, M.; Persson, P. Diastereomerization Dynamics of a Bistridentate Ru<sup>II</sup> Complex. *Inorg. Chem.* **2016**, *55*, 3015–3022.
- (48) Wadman, S. H.; Lutz, M.; Tooke, D. M.; Spek, A. L.; Hartl, F.; Havenith, R. W. A.; van Klink, G. P. M.; van Koten, G. Consequences of N<sub>2</sub>C<sub>2</sub>N- and C<sub>2</sub>N<sub>2</sub>N-Coordination Modes on Electronic and Photophysical Properties of Cyclometalated Aryl Ruthenium(II) Complexes. *Inorg. Chem.* **2009**, *48*, 1887–1900.
- (49) Jäger, M.; Smeigh, A.; Lombeck, F.; Görls, H.; Collin, J.-P.; Sauvage, J.-P.; Hammarström, L.; Johansson, O. Cyclometalated Ru<sup>II</sup> Complexes with Improved Octahedral Geometry: Synthesis and Photophysical Properties. *Inorg. Chem.* **2010**, *49*, 374–376.
- (50) Wilson, G. J.; Will, G. D. Density-Functional Analysis of the Electronic Structure of Tris-bipyridyl Ru(II) Sensitizers. *Inorg. Chim. Acta* **2010**, *363*, 1627–1638.
- (51) Osterman, T.; Abrahamsson, M.; Becker, H.-C.; Hammarström, L. Influence of Triplet State Multidimensionality on Excited State Lifetimes of Bis-tridentate Ru<sup>II</sup> Complexes: A Computational Study. *J. Phys. Chem. A* **2012**, *116*, 1041–1050.
- (52) Adamo, C.; Barone, V. Toward Reliable Density Functional Methods Without Adjustable Parameters: The PBE0 Model. *J. Chem. Phys.* **1999**, *110*, 6158–6170.
- (53) Perdew, J. P.; Ernzerhof, M.; Burke, K. Rationale for Mixing Exact Exchange with Density Functional Approximations. *J. Chem. Phys.* **1996**, *105*, 9982–9985.
- (54) Dolg, M.; Wedig, U.; Stoll, H.; Preuss, H. Energy-Adjusted Ab Initio Pseudopotentials for the First Row Transition Elements. *J. Chem. Phys.* **1987**, *86*, 866–872.
- (55) Tomasi, J.; Mennucci, B.; Cammi, R. Quantum Mechanical Continuum Solvation Models. *Chem. Rev.* **2005**, *105*, 2999–3094.
- (56) Persson, P.; Knitter, M.; Galoppini, E. Light-Harvesting and Electronic Contacting Capabilities of Ru(II) IPA Rod and Star Complexes - First Principles Predictions. *RSC Adv.* **2012**, *2*, 7868–7874.
- (57) Frisch, M. J.; Trucks, G. W.; Schlegel, H. B.; Scuseria, G. E.; Robb, M. A.; Cheeseman, J. R.; Scalmani, G.; Barone, V.; Mennucci, B.; Petersson, G. A.; et al. *Gaussian 09 Revision D.1*; Gaussian Inc.: Wallingford, CT, 2009.
- (58) Nocedal, J.; Wright, S. J. *Numerical Optimization*; Springer: New York, 2006.
- (59) Jones, E.; Oliphant, T.; Peterson, P. Others, SciPy: Open Source Scientific Tools for Python. <http://www.scipy.org/> [online; accessed 2016-03-02].
- (60) Nazeeruddin, M. K.; De Angelis, F.; Fantacci, S.; Selloni, A.; Viscardi, G.; Liska, P.; Ito, S.; Takeru, B.; Grätzel, M. Combined Experimental and DFT-TDDFT Computational Study of Photoelectrochemical Cell Ruthenium Sensitizers. *J. Am. Chem. Soc.* **2005**, *127*, 16835–16847.